LA-UR-24-25951

Approved for public release; distribution is unlimited.

Title:	Aquarium Shot Image Analysis
Author(s):	Nelson, Matthew Aaron Halverson, Scot Srinivasan, Gowri
Intended for:	Report
Issued:	2024-06-18

Aquarium Shot Image Analysis

Matthew Nelson, Scot Halverson, and Gowri Srinivasan*
D-3, Los Alamos National Laboratory, Los Alamos, New Mexico 87545
(Dated: August 5, 2013)

Quantitative analysis of fast-frame imagery of explosive aquarium shots can extract an abundance of information regarding the evolution of both the shock and the product gases following the passage of a detonation front. Analysis of the product gases (or any other surface of interest that lies within the shock and is observed from outside of the shock) is complicated by the fact that the water shock refracts the light in all three dimensions. This makes it necessary to correct for this refraction in order to get an accurate perception of the location of the surface and subsequently the velocities derived from the shape of that surface.

I. INTRODUCTION

The behavior of high explosive (HE) materials is typically characterized by detonating a cylinder of the HE at one end and observing the propagation of the detonation front and resulting shock wave. Fast-frame imagery is used to capture successive images during the detonation of the HE cylinder. It is desirable to use this fast-frame imagery for quantitative data analysis of the velocities produced during the detonation of the HD cylinder in addition to the qualitative understanding of the detonation process that can be obtained through the fast-frame imagery observations. This paper details the process used to analyze the fast-frame imagery and extract velocity information from it.

II. EXPERIMENTAL DETAILS

An aquarium shot uses a cylinder of HE submerged within a transparent tank of water. This makes it possible to observe both the resulting shock wave and the product gases that are produced from the detonation process. These shots employ an HE cylinder that is 2 inches in diameter and 9 inches in length. The shot data used to demonstrate the velocity calculations was acquired on 8/11/2011. This data was used because it had the best image quality of all of the aquarium tests.

III. DETONATION VELOCITY CALCULATION

The detonation velocity (the rate at which the detonation front travels down the HE cylinder) is calculated using a simple difference in undetonated length of the HE cylinder between images and dividing the difference in length by the time delay between the images. The image is scaled by the user defining the left and right sides of the unexploded HE cylinder on the image and specifying the diameter of the cylinder. Using sequential images produces the blue line in the plot of detonation velocity in FIG. 2.

The variation of detonation velocity using this method is non-physical. If it were physical, there would be evidence of it in the shape of the shock wave producing bumps in the profile. Observing the smooth nature of the shock surface it is obvious that the detonation process must also be smooth and steady. Instead, these jumps in the detonation velocity measurement are due to errors in the graphical measurement of the length of undetonated material and the differential nature of the calculation amplifies the inherent inaccuracies resulting in large fluctuations in the measured detonation velocity. Since the detonation process ideally occurs at a constant rate, measuring the detonation velocity over the entire shot will provide a much more accurate value of 7.65 km/s.

IV. REFRACTION CORRECTION

The phase (shock and product gases) and/or surface (pipe) profiles are derived from data points that are graphically defined by the user in the graphical user interface (GUI). A third-order polynomial fit of these data points is then used for analysis in order to provide a smooth and easily differentiable curve. Note that the shock interface produces a magnification effect due to the difference in the index of refraction between the shocked and unshocked water. The profile of the surfaces which are inside the shock must be corrected in order to get an accurate estimate of the velocities.

A. Method

The profile of the product gases as seen in the 2D fast-frame image, e.g., FIG. 1,is distorted in all three dimensions due to the light passing through the 3D shock surface. FIG. 3 shows a ray of light (shown in blue) emitted from the back face of the product gas surface will be bent as it comes into contact with the shock surface to give a false perception of the axial, radial, and rotational positions of the profile. This explains the sudden apparent expansion of product gases near the detonation front in the fast-frame images as seen in FIG. 1.

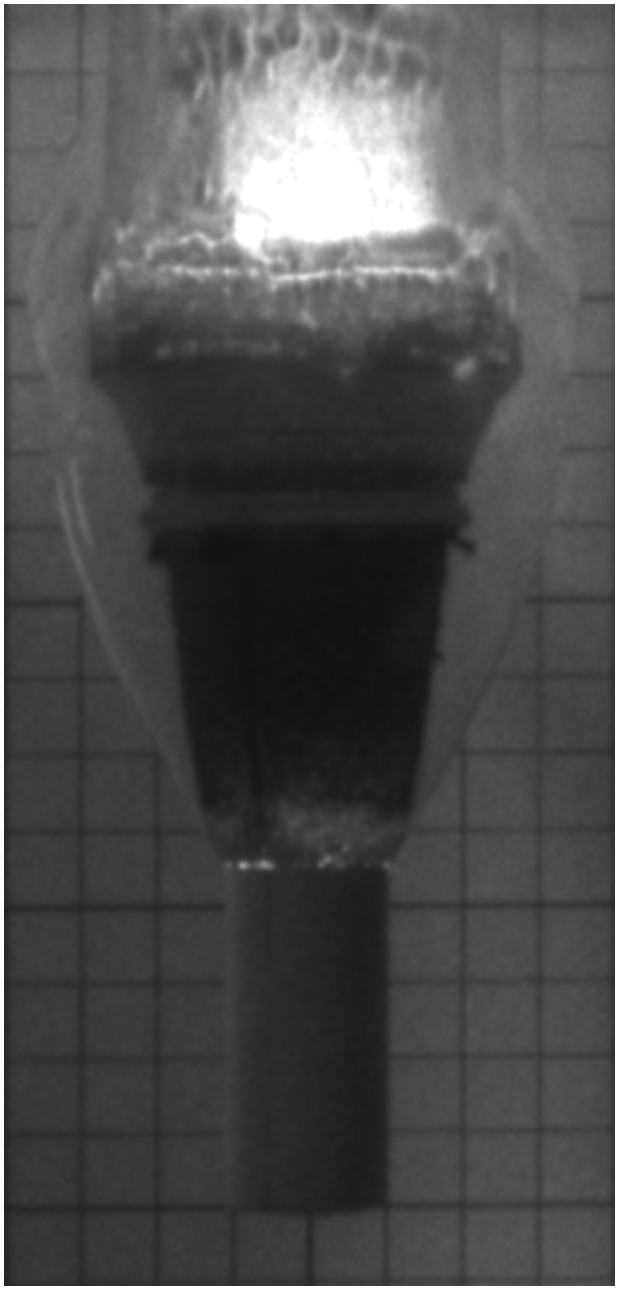

FIG. 1: Sample aquarium shot image.

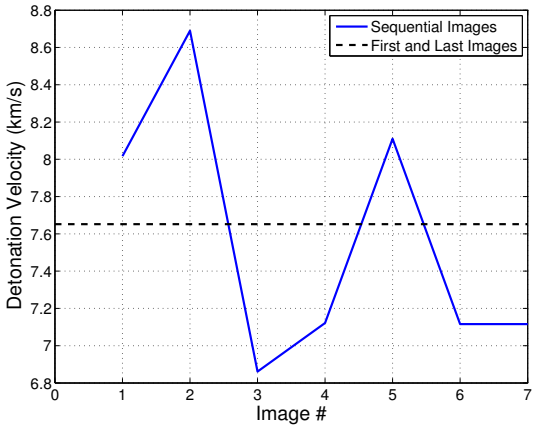

FIG. 2: Detonation velocity as measured by sequential images (blue) and the first and last image (black).

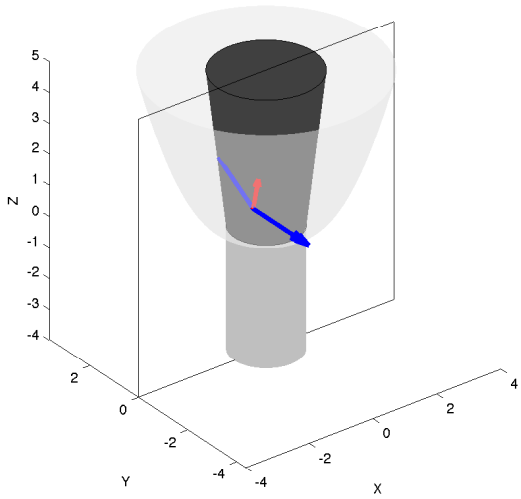

FIG. 3: 3D view of the refraction process that occurs due to the shocked water.

FIG. 4 shows this process in 2D for illustrative purposes. $\vec{N}$ is the outward surface normal unit vector. $\vec{I}$ is the unit vector of the incident ray. $\vec{T}$ is the unit vector of the transmitted ray. The incident ray of light will bend as it travels obliquely into the local plane of the interface between two mediums of different densities (ρ_1 and ρ_2) and therefore different indices of refraction (n_1 and n_2). For the example shown in FIG. 4 illustrates the refraction process when the light passes into a medium that is more dense (i.e., $\rho_1 < \rho_2$ and $n_1 < n_2$) therefore $\theta_1 > \theta_2$ according to Snell's law:

$$n_1 sin(\theta_1) = n_2 sin(\theta_2)$$

There are several steps in the refraction correction process. First, we assume that the shock surface is axisymmetric so the profile measured at the side of the shock surface can be rotated to find the local surface normal unit vector. We determine the rotation angle around the axis of the cylinder of the interior profile point by taking the inverse cosine of the ratio of the projected radial position (r_p) to the radial position (r) of the shock profile at the axial position (z) of the user defined data point.

Now to simplify the calculation we convert the surface

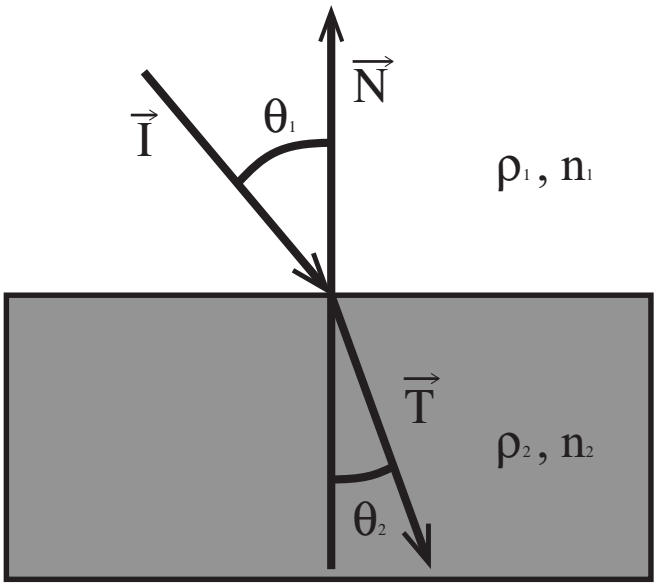

FIG. 4: 2D view of the refraction process that occurs due to a ray of light traveling through the interface of two mediums with different densities and therefore indices of refraction.

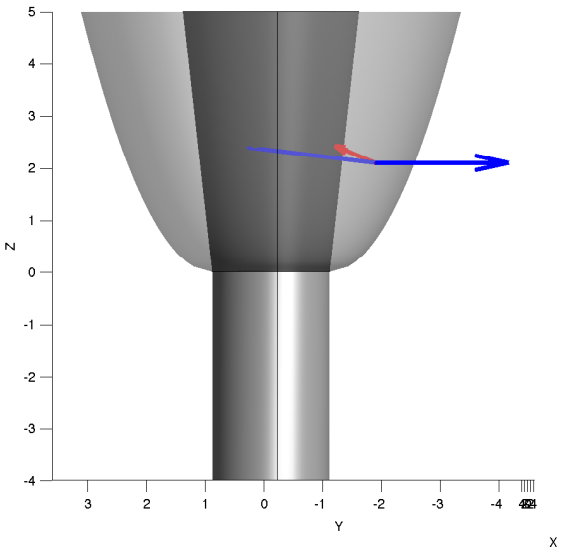

FIG. 6: Side view of the refraction process that occurs due to the shocked water.

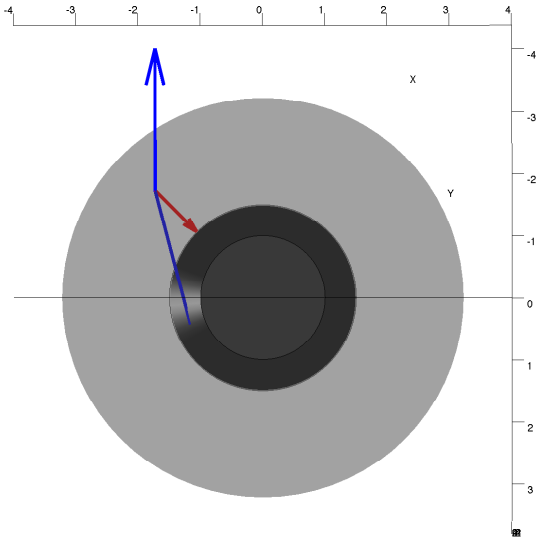

FIG. 5: Bottom view of the refraction process that occurs due to the shocked water.

normal unit vector in the plane of the image into Cartesian coordinates and rotate it around the cylinder axis to find the local surface normal unit vector at the point of intersection. We also assume that the light is effectively parallel when it arrives at the camera, i.e., that it leaves the shock surface in a direction normal to the plane of the image. In addition we solve the ray tracing problem backwards since we know the direction that the ray travels once it leaves the shock rather than the point of origin, which is what we are trying to determine.

Once we have the incident ray direction (assumed to be perpendicular to the image surface) and the local shock surface normal unit vector, we can then employ Heckbert's 3D refraction method [1] to find the direction from which the ray originated.

$\vec{N}$ is 3D surface normal unit vector. $\vec{I}$ is the 3D unit vector of the incident ray. $\vec{T}$ is the 3D unit vector of the transmitted ray. The indices of refraction are n_1 (for the material that the light is traveling from) and n_2 (for the material that the light is traveling to). In this case, since we will solve this problem in reverse, n_1 will be that of unshocked water, which has a value of 1.333. According to Zel'Dovich and Raizer [2] the index of refraction for shocked water is 1.46 ± 0.03 when measured using reflective methods and 1.49 ± 0.03 when measured using geometric methods. In the absence of any evidence indicating which method is a more accurate measure of the index of refraction we have elected to use the mean value of the two methods, i.e., 1.475, to correct for refraction in our analyses.

$$\eta = \frac{n_1}{n_2}$$

$$C_1 = -\vec{N} \bullet \vec{I}$$

$$C_{S2} = 1 - \eta^2(1 - C_1^2)$$

C_1 is simply $cos\theta_1$ shown in FIG. 4. C_{S2} is $cos^2\theta_2$, the relation shown above is derived from Snell's law and trigonometric relationships. Snell's law and the Pythagorean theorem are then used to derive the final relationship to calculate the $\vec{T}$ from $\vec{N}$, $\vec{I}$, and η.

$$\vec{T} = \frac{\eta\vec{I} + \left(\eta C_1 - \sqrt{C_{S2}}\right)\vec{N}}{\left|\eta\vec{I} + \left(\eta C_1 - \sqrt{C_{S2}}\right)\vec{N}\right|}$$

If C_{S2} is less than 0 then there is total internal reflection. Otherwise a portion of the ray will be reflected and the rest will be refracted and transmitted into the material. Because we are only interested in the direction of refraction, we normalize the resulting vector to produce a unit vector that defines the transmission direction.

Once we have the direction of the transmitted vector we can solve for the radial component by determining the minimum distance between two lines: the transmitted ray and the cylinder axis.

$\vec{Z}$ is the z axis unit vector. $\vec{P}$ is the point of incidence position vector. $\vec{O}$ is the origin position vector. First find the common perpendicular direction vector ($\vec{C}$) by taking the cross product of $\vec{T}$ and $\vec{Z}$:

$$\vec{C} = \frac{\vec{T} \times \vec{Z}}{\left|\vec{T} \times \vec{Z}\right|}$$

Then determine the direction vector ($\vec{D}$) between the two reference points:

$$\vec{D} = \vec{P} - \vec{O}$$

Finally the minimum distance (r) between the lines is simply:

$$r = \vec{C} \bullet \vec{D}$$

Finally, once the corrected radial position of the point is known, we can solve for the corrected axial position of the point of interest. Start with the vector definition of the transmitted line ($\vec{L}$) starting at the point of incidence:

$$\vec{L} = \vec{P} + S\vec{T}$$

The axial position is found iteratively by solving for the distance (S) along the line that will produce a radial position equal to the minimum distance (r). Once we have found S then we can solve for the corrected axial position (z) by using the axial component of $\vec{L}$.

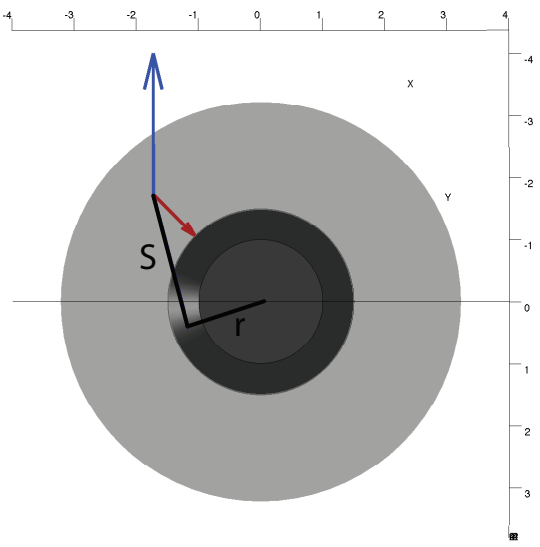

FIG. 7: Diagram of the physical significance of the quantities used to determine the corrected position of the interior profile points.

B. Image Analysis

Using the image found in FIG. 1 the user graphically selects characteristic points to define both the shock and the interior profile (i.e., contact discontinuity of water and explosive product gases) as is seen in FIG. 8.

The profile points are translated into a cylindrical coordinate system based on the moving detonation front and the axis of the cylinder. In the absence of any information regarding the aquarium glass and its surface normal vector we assume that any distortion of the observed image due to the aquarium glass is negligible. We therefore assume that the shock profile is as it appears in the image and we use a polynomial fit to the shock profile data to correct for the refraction on the observed position of the product gas data points. Applying the above mentioned refraction correction to all of the profile points of all of the frames superimposed on to the same plot we get the profiles shown in FIG. 9.

In examining the corrected product gas profile position shown in FIG. 9, a few noteworthy aspects become apparent: First, the apparent discreet expansion of the product gases is indeed simply an optical illusion due to the refraction of the light as it passes through the water shock. Second, the polynomial fit to the corrected gas product profile gives us confidence in the value of the index of refraction that was used in the refraction correction algorithm because without forcing or nudging (by adding an assumed profile point at the unexploded radius and the detonation front) the corrected profile smoothly meets the shock profile at the detonation front as one

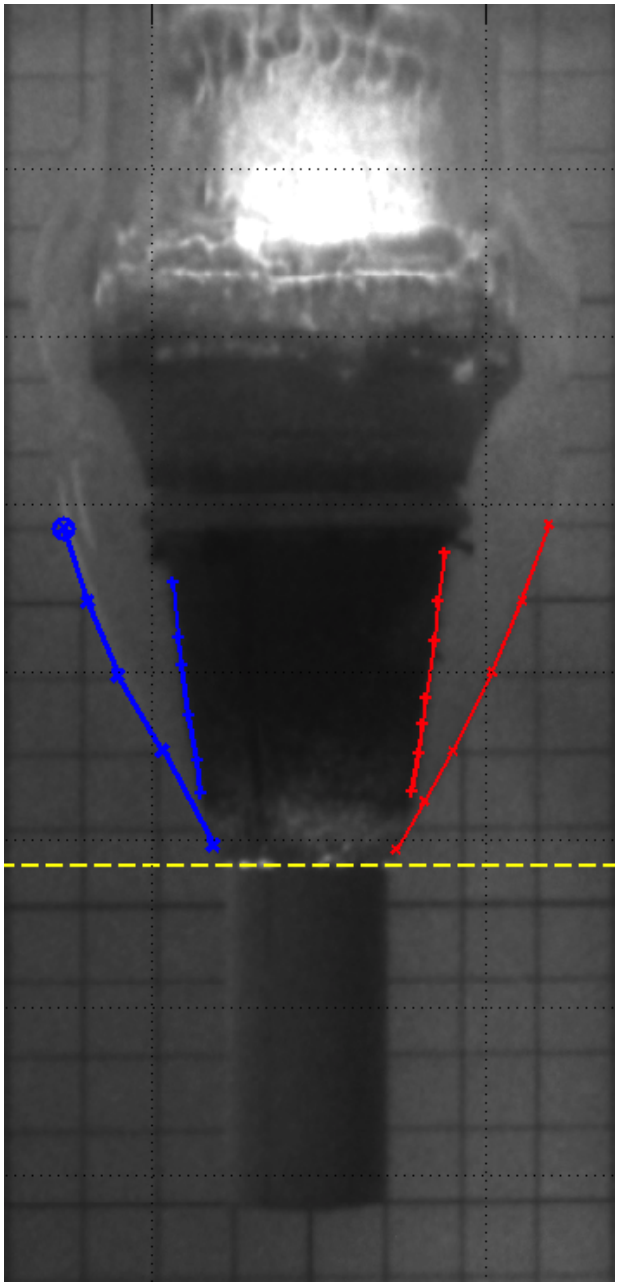

FIG. 8: Sample aquarium shot image with user defined shock and product gas profiles.

would expect. Third, while the agreement between the two sides of the image is quite good there is still some variability due to the inconsistencies inherent in the user defined data point selection process. It is therefor desirable to take advantage of the quasi-steady-state nature of the detonation process and use an ensemble average of all of the profiles from an experimental shot rather than those from a single image to reduce the statistical uncertainty in the polynomial fit to the profile data. Using the profiles from all of the fast-frame images we are able to produce the fits shown in FIG. 10. It is readily apparent

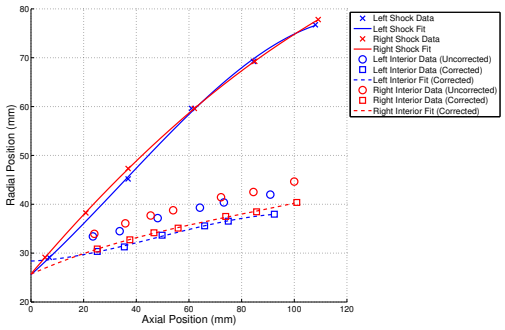

FIG. 9: Shock and product gas profiles from the image shown in FIG. 8.

from this plot that the quasi-steady-state assumption is remarkably accurate in that all of the individual profiles fall right on top of each other.

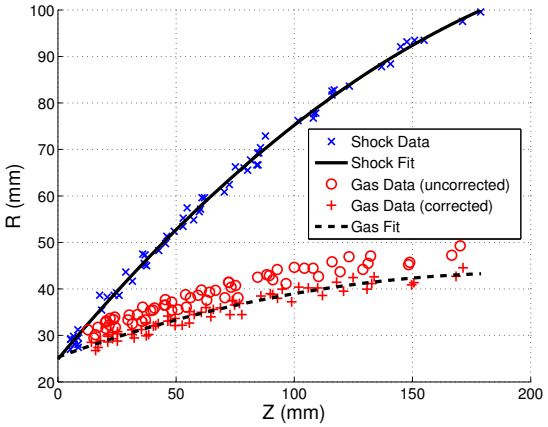

FIG. 10: Shock and product gas profiles from all images of the example aquarium shot.

As an independent means of verification of the refraction correction algorithm we have employed POV-Ray ray tracing software to render computer generated images of the aquarium shot using the polynomial curve fits shown in FIG. 10 to define the shock and product gas surfaces. FIG. 11 shows what the aquarium shot would look like without the distortion caused be the refraction at the shock surface, i.e., if the shocked and undisturbed water had the same index of refraction. The transparency of shock surface has been reduced in order to make it visible in this rendering due to the fact that it is actually the refraction at the shock surface that makes it visible. FIG. 12 is the computer generated image of the example aquarium shot using the proper indices of refraction for shocked and undisturbed water. Note that including the refraction has replicated the apparent sudden expansion of the product gases near the detonation front observed in FIG. 1.

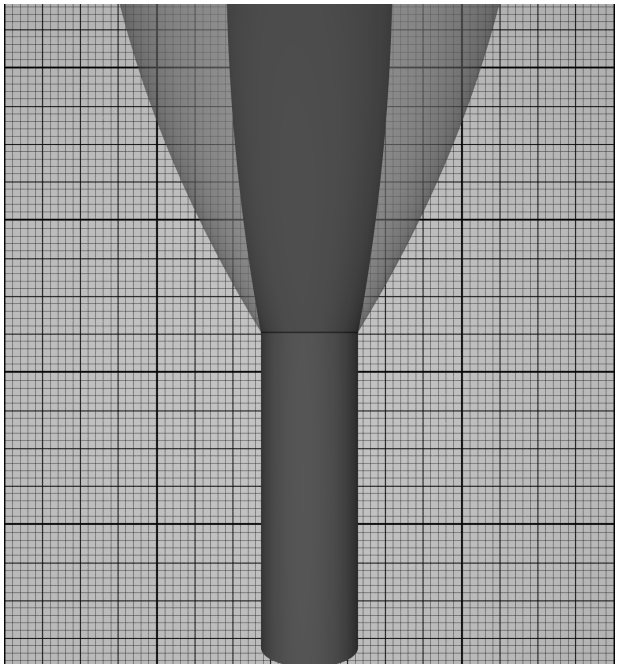

FIG. 11: A 3D rendering of the example aquarium shot using an index of refraction ratio of 1.

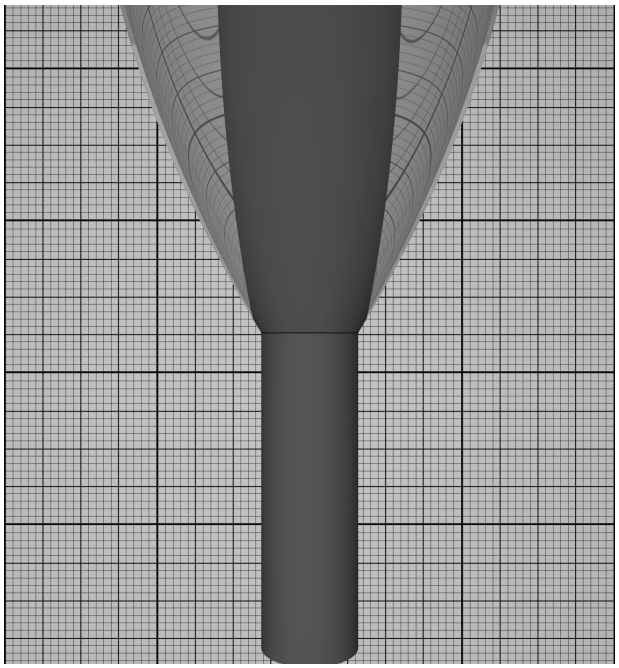

FIG. 12: A 3D rendering of the example aquarium shot using an index of refraction ratio of 1.475/1.333.

V. AUTOMATED IMAGE ANALYSIS

The polynomial fit calculations and subsequent calculations are highly dependent on the accuracy and consistency of the data manually entered by the user. Manually determining data points is prone to error and is time consuming. We developed two automated systems to overcome the problems with manual image processing. However, these systems are not perfect, and can produce incorrect results. As a result, the user has the ability to override the automatic systems by manually correcting the image and detecting curve locations.

A. Rotation and Line Detection

The first system is designed to automatically determine any image rotation correction, as well as where vertical and horizontal lines of interest appear within the image. These operations are performed on individual images in the set. The vertical lines include the left and right edges of the unexploded HE, and the horizontal lines include the detonation front and a reference line consistent between images.

The detection of vertical and horizontal lines is performed using a sequence of image processing and analysis techniques, including Canny[3] and Sobel[4] Edge detection, as well as a Hough Line Transform[5]. The success of subsequent image analysis is dependent on correct image rotation, and the success of the image rotation calculation is dependent on the ability to detect horizontal and vertical lines of interest. As a result, there is a mutual dependency between rotation calculation and line detection. This is handled by performing rotation and line detection as an iterative process that is repeated multiple times. FIG. 13 shows the end result of the automated image rotation and line detection algorithms.

1. Rotation

Image rotation is calculated using a Hough Line Transform. A Hough Transform is a means of determining parameters for an equation that is to be detected in an image. In our case, the Hough Transform is used to detect the parameters of a set of lines. In particular, the Hough Transform is used to detect the distance from the origin and the angle of a line. In order to accomplish this, an edge detection algorithm is used to detect points of interest within the image. This is accomplished by first blurring the image using a Difference of Gaussians filter, and then running Sobel Edge detection on the resulting image. This produces a binary image, with pixels representing points of interest set to 'on'. For each of these pixels, a range of possible origin offsets are used to calculate a set of lines that could include the pixel. A value representing the offset and angle is incremented, and the process is repeated for all 'on' pixels in the image. This results in a two dimensional set of sums representing the set of possible line parameters in the image and their associated relative probabilities. FIG. 14 shows a subset of a Hough Line Transform for the HE shot image shown in

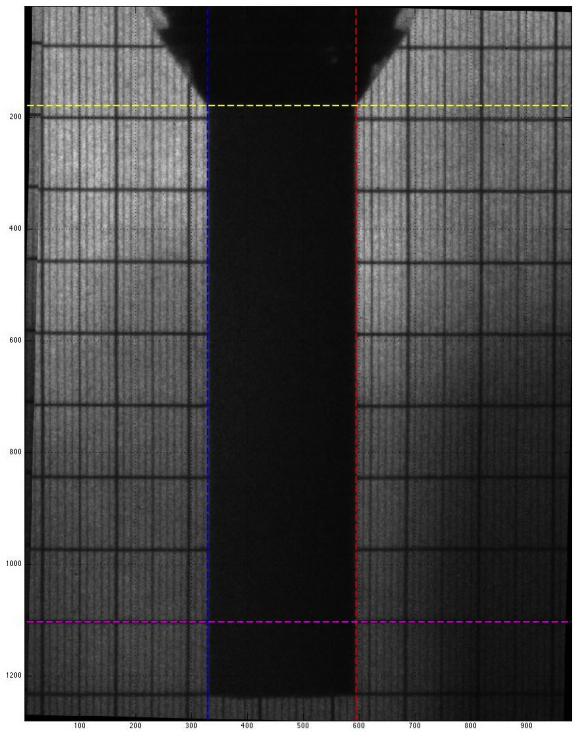

FIG. 13: Detected lines superimposed on a rotation corrected image

FIG. 14: Hough Line Transform for HE Shot Image

FIG. 13. The vertical axis shows the distance from the origin in pixels, and the horizontal axis shows the angle of rotation in the range $[-5° : 5°]$ in .1° increments. The darkest spots correspond to the most commonly matched parameters. Note that the darkest regions are slightly left of center vertically, corresponding to a slight negative rotation. In this case, the rotation angle was -1.3°.

While the Hough Line Transform produces probabilities for both parameters of the line equation, we're only interested in the probabilities of the line angle. Thus, the the probabilities for all lines with a particular angle are summed together, producing a one dimensional array of angle probabilities. Assuming vertical lines are predominant in the original image, the most probable angle resulting from the Hough Line transform should correspond to the angle by which the image is rotated. Rotating the image by the same amount in the opposite direction should result in a rotation corrected image.

Particularly for images appearing towards the end of a HE shot sequence, vertical edges are hard to detect because the region of HE beyond the detonation front tends to be relatively small. This makes rotation detection difficult. Fortunately, the angle of rotation for an image tends to be consistent within a shot sequence. In order to handle poor rotation detection in these images, the average rotation of previous images in the sequence is calculated, and the final image rotation is calculated as a weighted function of how far the detonation front has progressed, the average rotation of previous images, and the rotation calculated by the Hough Line transform.

2. Vertical Lines

Once an initial rotation angle has been calculated and the image corrected to accound for it, the vertical edges of the HE stick are calculated. In order to detect these edges, the rotated and edge detected image previously produced in the rotation calculations is used to produce a vertical histogram. The histogram contains counts of pixels of interest along vertical columns in the image. It is assumed that the HE stick is roughly centered in the image. Given this assumption, the vertical edge detection algorithm walks left and right from the center of the histogram, ignoring values until a threshold is crossed. Once the threshold has been crossed, the algorithm will continue until the next point on the histogram contains fewer points of interest than the current point. This point is assumed to correspond to the left or right edge of the HE stick, depending on the direction in which the algorithm is walking.

3. Horizontal Lines

In order to determine the detonation front, a horizontal histogram is created from the edge detected image

generated in the rotation detection code. The histogram is generated only from the region between the detected left and right edges of the HE stick, and ignores the top and bottom 100 rows of pixels. Because the detonation front usually corresponds to a slight change in image intensity, the rows of pixels along the detonation front will likely contain more points of interest than any other rows. Thus, the row with the highest value in the histogram likely corresponds to the detonation front.

A horizontal reference line is determined in a similar fashion. A horizontal histogram of a small region in the lower half of the edge detected image is generated, and the horizontal line with the greatest value is assumed to correspond to a horizontal line of interest.

B. Curve Detection

The process of line detection and image rotation primarily serves as preprocessing for curve detection. The process for detecting the explosive shock and expanding gas curves is dependent on the results of the vertical and horizontal line detection performed on all user accepted images in the shot sequence. As such, it is necessary to perform this step after all the images in the sequence have been rotated and processed for line detection.

The set of images accepted by the user is used to compute curves for the shock wave and the expanding gasses. However, the images tend to be noisy, and finding distinct edges in a noisy image is difficult. To account for this, the regions of interest for the curves are aligned and processed individually. Then the set is merged together to produce one image representative of all accepted images in the sequence. Edge detection is used on the merged image, producing a set of edge points within the image. These points are then grouped into adjacent sets that are representative of curves. A polynomial equation is then fit to the points for each of the curves.

For each image in the sequence, the image is cropped into two regions of interest. One to the left of the left edge of the HE stick and above the detonation front, and the other to the right of the right edge of the HE stick and above the detonation front. These two regions represent the left and right curve regions of the image. The right image is flipped about the Y axis so as to overlap with the left, and then both images are rotated 90 degrees so that the curves in the image correspond to a function of the X axis. The image contrast is increased to bring out noticable edges, and then Canny edge detection is performed on each image, and small regions of noise are removed. Once again, edge detection produces a binary image, with points of interest set to 'on', or a value of 1.

The set of images are then merged together, summing the results into one image. The data in this image is then scaled to the range $[0:1]$. The result can be seen in FIG. 15. Canny edge detection is then performed again on this single image. Horizontal and vertical lines are then removed and the resulting image is blurred and denoised. This results in an image that is primarily composed of two distinct curves averaged over the set of images accepted by the user. From here, a skeleton morphological operation is performed to shrink the edges to single pixel thickness where possible.

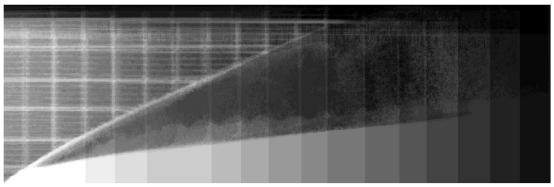

FIG. 15: Merged set of edge detected regions of interest

Finally, the resulting image is split into groups of adjacent and near adjacent pixels. The image is processed from right to left, grouping pixels that are within some threshold of eachother vertically. Of this set of groups, the two with the largest number of pixels is identified and the average slope for each calculated. The group with the steeper slope is assumed to be the shock curve and the shallower slope is assumed to be the gas curve. From here, the separated groups of points are used in a polynomial fit equation to produce a set of parameters representing a best fit curve. FIG. 17 shows two third-order polynomials fit to the shock and gas profiles.

VI. SLIT VELOCITY CALCULATION

The slit velocity (U_{slit}) is derived from a measurement method which employs a slit camera that tracks the time history of the radial expansion of a surface or phase at a set axial position along the cylinder during the detonation of a cylinder test. Menikoff et al. [6] use the quasi steady-state assumption to derive the functional relationship between the slope of the profile and U_{slit} as follows:

$$U_{slit} = \left|\frac{dr}{dz}\right| D$$

Where D is the detonation velocity and $\frac{dr}{dz}$ is the local slope of the profile curve. Due to the quasi steady-state nature of the detonation process it is also possible to convert the axial positions relative to the detonation front into an elapsed time from the passage of the detonation front at that axial position through the following relation:

$$t = \frac{z}{D}$$

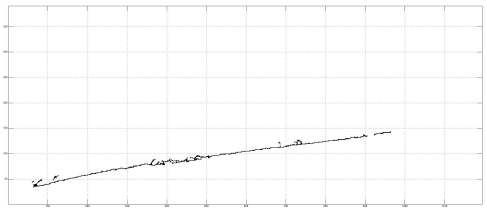

(a) Detected Gas Curve Edge

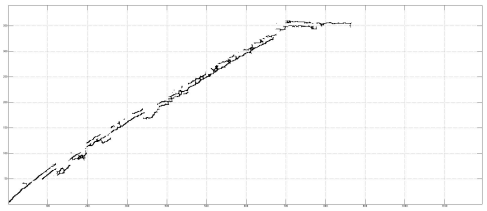

(b) Detected Shock Curve Edge

FIG. 16: Plots of Points Separated into Shock and Gas Plots

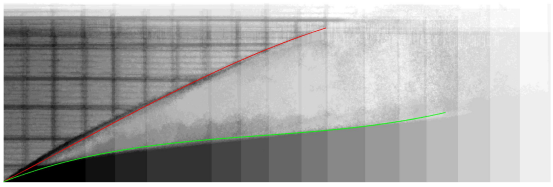

FIG. 17: Merged set of edge detected regions of interest

The use of a polynomial fit to the data makes it very simple to determine the slope of the profiles through a simple differentiation of the polynomial equation for the fit. Then employing the relation between slope and U_{slit} and the conversion from spatial into time we can produce the following plot of the resulting shock and product gas slit velocities. in FIG. 18. The speed of sound in unshocked water is approximately 1.48 km/s and the speed of sound can be expected to be faster in shocked water due to the higher density. As one would expect, the shock travels faster than the speed of sound, while the product gases, which are located on the other side of the shock wave, travel at speeds below the speed of sound in the medium.

VII. CONCLUSIONS

Using ray-tracing techniques in combination with geometrical relations in a quasi steady-state detonation process, it is possible to get quantitative measurements of the

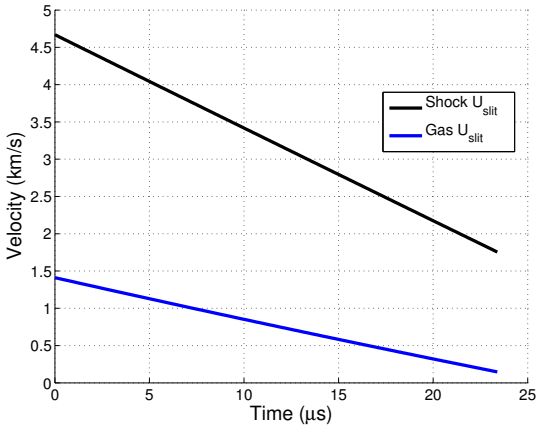

FIG. 18: Shock and product gas slit velocities based on all of the images of the example aquarium shot.

velocities produced through the detonation of a cylinder of HE from fast-frame imagery. Overlaying the successive images on top of each other demonstrated the quasi steady-state nature of the detonation process. The shock refraction correction makes it clear that the observed rapid expansion of the product gases near the detonation front was merely an optical illusion resulting from the refraction at the shock surface. The observed profile locations are distored in all three dimensions. The actual profile of the product gases expands smoothly from the unexploded HE cylinder radius at the detonation front to the shape of the curve that is observable through the shock.

* nelsonm@lanl.gov

[1] A. S. Glassner, ed., *An Introduction to Ray Tracing* (Morgan Kaufmann, San Francisco, CA, USA, 1989).

[2] Y. B. Zel'Dovich and Y. P. Raizer, *Physics of Shock Waves and High Temperature Hydrodynamic Phenomena* (Dover Publications, Inc., Mineola, NY, USA, 2002).

[3] J. Canny, IEEE Trans. Pattern Anal. Mach. Intell. **8**, 679 (1986), ISSN 0162-8828, URL http://dx.doi.org/10.1109/TPAMI.1986.4767851.

[4] W. Gao, X. Zhang, L. Yang, and H. Liu, in *Computer Science and Information Technology (ICCSIT), 2010 3rd IEEE International Conference on* (2010), vol. 5, pp. 67–71.

[5] R. O. Duda and P. E. Hart, Commun. ACM **15**, 11 (1972), ISSN 0001-0782, URL http://doi.acm.org/10.1145/361237.361242.

[6] R. Menikoff, C. A. Scovel, and M. S. Shaw, Tech. Rep. LA-UR-13-23630, Los Alamos National Laboratory, Los Alamos, NM, USA (2013).